Non-invasive Mechanism Classification and Localization in Supraventricular Cardiac Arrhythmias

I Sandoval[1], VG Marques[2], JA Sims[1], M Rodrigo[3], MS Guillem[4], J Salinet[1]

[1] Biomedical Engineering, Engineering, Modelling and Applied Social Sciences Center, Federal University of ABC, São Paulo, Brazil
[2] Physiology Department, Maastricht University, Maastricht, Netherlands
[3] Universitat de València
[4] Universitat Politècnica de València

Abstract

In this study, we investigated the most relevant biomarkers for noninvasive classification and mechanism location in atrial tachycardia (AT), flutter (AFL) and fibrillation (AF). Biomarkers were calculated using noninvasive body surface (BSPM) dominant frequency and phase maps. We used 19 simulations of 567 to 64-lead BSPMs, from which were extracted 32 biomarkers. Biomarker ranking was performed with ANOVA, Kendall and Lasso techniques. The best four biomarkers were identified and used to classify the arrhythmias in all combinations, and the best two used for noninvasive driver localization. Arrhythmia classification accuracy was 94.74%. The feature combination which best distinguish AF from non-AF were mean filament displacement and mean OI, while those that best distinguish AFL from AT were mean and SD of SP distribution. There was good agreement across ranking techniques. Mechanism location accuracy was 78.95%, with the most important biomarkers being percentage SPs within each torso division, and SD of filament histogram cluster area. This study highlights that organization related features well identifies AF and spatial SP distribution discriminate AT from AFL and also it's localization.

1. Introduction

The three most common cardiac arrhythmias in clinical practice are atrial tachycardia (AT), flutter (AFL) and fibrillation (AF) [1]. There are different mechanisms responsible for triggering and maintaining these arrhythmias: for AT, a set of localized cells fire radially in a regular high frequency rhythm, ectopic focus [1]; AFL also has a regular high frequency rhythm, but here the wavefront depolarization propagates as a macroreentry, usually around the valves or fibrosis [2]; in contrast to the previous supraventricular arrhythmias, AF is characterized by uncoordinated high frequency atrial activations, with consequent deterioration of mechanical function, and the presence of functional rotors [3]. This arrhythmia is the most common cardiac arrhythmia found in clinical practice, affecting around 2% of the adult worldwide population [3]. Since the efficiency in the atrial systolic and diastolic functions are compromised, cardiac output decreases, leading to occurrences of thromboembolic phenomena, heart failure and sudden arrhythmic death [4].

Currently, radiofrequency catheter ablation is used to treat these three arrhythmias, which has been shown to be safe and effective. But for some groups of patients, especially those with persistent AF, outcomes are nonsatisfactory, and procedures might need to be repeated [5]. In this intervention, a catheter, containing one or more electrodes, is introduced into the atria. Contact is made with the endocardium, resulting in radiofrequency cauterization to the predefined areas, which has the aim of preventing the mechanisms through elimination of their electrical activity [6]. This method depends on accurate location of the driving mechanism, which is routinely performed with invasive electrical mapping of the atrium [7], which increases the duration of the surgical procedure. We hypothesize that classification and location of cardiac arrythmias might be obtained non-invasively, calculated from high density body surface dominant frequency (DF) and phase maps. If so, these could be useful auxiliary tools for clinicians planning therapeutic strategies prior to invasive procedures.

2. Methodology

A computational model of the atrium composed by 284578 nodes was used to simulate the electrical behavior of the left (LA) and right atria (RA) in the three arrhythmias. A total of 19 simulations were used, each of which shows an arrythmia originating in one of the three distinct

mechanisms: AT (4 simulations), driven by an ectopic focus; AFL (4 simulations), driven by a macro-reentrant circuit; AF (11 simulations), driven by functional rotors [8]. The ectopic foci in AT models were generated by applying pulse trains with a constant frequency on nodes inside the regions of interest [9], while AFL and AF signals were generated by introducing atrial remodeling in the regions of interest. The remodeling was simulated by shortening the duration of the action potential duration and decreasing diffusion in cardiac tissue, which induces rotational activity [8,10]. The system of differential equations in the atrial cell model was solved using Runge-Kutta integration. AFL simulations induced macro-reentry around anatomic structures (tricuspid valve, inferior vena cava and pulmonary veins), while AF was driven by functional rotors in the specific locations.

2.1. Preprocessing and lead layouts

Body surface potential maps were obtained by solving the forward problem with the boundary element method, through a uniform torso, of 771 data points and sampled at 500 Hz [2, 8]. From this, a reduced number of points were selected to represent different lead layouts. The number of leads varied from 567, the highest resolution (HR), to a lowest resolution (LR) of 64 lead, in a total of 5 different acquisition layouts, allowing an impact analysis of reducing the number of leads, and consequently the reduction of the spatial resolution. White Gaussian noise was also added to the BSPM signals with a signal-to-noise ratio (SNR) of 10 [2]. The coordinates of the BSPM nodes in the models went through a cylindrical projection, which were interpolated into a 30 by 65 grid using cubic splines [2].

2.2. DF maps

DFs were calculated using a previously validated method, based on the continuous wavelet transforms [11]. DF maps were used to calculate 6 biomarkers: (i) DF mean (DF-*M*); (ii) median (DF-*Mdn*); (iii) mode (DF-*Mo*), (iv) highest DF (HDF); (v) inter-quartile range (IQR) and; (vi) mean DF and HDF ratio (DF-*M*/HDF). From *HDF* regions (HDFr), where $|DF - HDF| \leq 1Hz$. Seven features were calculated from HDFrs: (i) number of HDFr (DF-*N*r); (ii) average size (DF-*M*s); and (iii) standard deviation (SD, DF-*SD*s); (iv) the percentage of the total area of the potential map occupied by HDFr (DF-Ar); and (v) mean (DF-*MOI*); (vi) SD (DF-*SD*OI); and (vii) IQR (DF-IQROI) of the organization index (OI) [12]. To avoid DFs related to harmonic activity or noise, which could impair the atrial HDF estimations and related biomarkers, the DF values above the 90th percentile were ignored.

2.3. Phase maps

In order to acquire the phase maps, a narrow 4th order Butterworth band-pass filter was applied to the BSPM signals in a range of 2 Hz around the HDF value, followed by the application of the Hilbert transform [13]. The phase angle was obtained by calculating the arc-tangent of the division of the Hilbert transformed signal by the original signal [2]. Signals were downsampled to 128 Hz to reduce processing time.

2.3.1. Rotor Detection

Rotational activity was detected by locating phase singularity points (SP), which were defined as points around which all phases converge [2, 14]. A Canny edge detector [15] was used to find discontinuities in the phase maps corresponding to shifts from $+\pi$ to $-\pi$, with the endpoints of the edges considered as possible SP. The analysis of these points was based on the phase of neighboring points, along rings with five different radii from 2 to 10 cm, and its phase values were obtained by interpolation, based on the 8 closest pixels values [8,10]. Criteria were developed to classify a point as an SP; the phase progression on at least two rings should satisfy the following: (i) the phase should progress in a minimum range of π; (ii) the progression should be ordered in at least 60% of its length; and (iii) there should be no phase discontinuities larger than π [8].

2.4. Spatiotemporal Analysis of Rotors

The SPs spatiotemporal distribution was analyzed based on filament maps and the heatmaps (HM), calculated through a 2D histogram of the filaments' SPs over time [11]. Then eight filament features were determined: (i) mean (Ph-*M*d); and (ii) SD of filament duration (Ph-*SD*d); (iii) mean (Ph-*Mf*); and (iv) SD of frequency of the rotation around SPs in the filaments (Ph-*SDf*); (v) average direction of rotation (+1 for clockwise and -1 for counterclockwise, Ph-*M*DR); (vi) filament rate over time (Ph-Fl*R*); (vii) mean (Ph-*M*FD); and (viii) SD filament spatial displacement (Ph-*SD*FD), defined as the average displacement in each sample, given by the Euclidean distance in subsequent frames.

From the HM, 11 biomarkers were obtained: (i) number of regions (Ph-*N*r); (ii) mean (Ph-*M*rs); and (iii) SD (Ph-*SD*rs) of region sizes (HMr); the area of each region was determined, A, as was the percentage of SPs in each region (pSP). From these, the following were obtained: (iv) mean (Ph-*M*SPA); and (v) SD of the value (Ph-*SD*SPA), for each region, of the ratio between pSP and A (pSPA); (vi) number of detected SPs over time (Ph-SPS); (vii) percentage of SPs (DF-pSP) in each of 4 subdivisions of the HM (only for mechanism localization) and; (viii) percent-

age of HMr area (Ph-HMrA). Moreover, HM is generated for each individual filament (HMi), and the following were calculated: (ix) the mean region size (Ph-HMiS); (x) mean SPs density (Ph-HMiD); (xi) mean area of the bounding box around each region (Ph-HMiB).

2.5. Feature ranking and classification

After computing the 32 features described above, feature ranking was performed using 3 different methods, then combined using the quadratic sum of the scores, normalized by the greatest value among features. The ranking was based only on the features obtained for HR layout and was performed aimed to the best features for discriminate: (i) AF from the others (AT and AFL); (ii) AT from AFL, and; (iii) its mechanism localization (LA or RA).

The first ranking method was based on analysis of variance's (ANOVA) f-score, which compares the ratio between the variance of the mean for each class and the variance of the entire dataset, meaning that higher values are indicative of a good classifier. The second method was based in Kendall's τ coefficient [16], which is a suitable correlation coefficient for both quantitative and qualitative variables. Finally, the third method was based on Lasso's (least absolute shrinkage and selection operator) regularization for logistic regression [17]. All ranking processes were performed with Scipy and Scikit-Learn libraries in Python 3. After feature ranking, the best four features for arrhythmia mechanism classification (MC) and two features for mechanism localization (ML) were selected, excluding redundant features, according to their Pearson correlation coefficient. This number of selected features was chosen to avoid overfitting, considering our dataset's size. For ML, all features were obtained for four overlapping divisions on the maps, referring to the left, right, front and back of the torso, resulting in eight features. The classifiers consisted in the logistic regression algorithm from Scikit-Learn, and the division of training and testing set was made using the leave-one-out method, a variation of k-fold for just one example in the test-set. Different combinations of the features among the pre-selected were also tested as inputs for the classifiers.

3. Results and Discussion

Figure 1 summarizes the ranking of the entire set of features with each respective combined score, normalized. In MC, DF-*M*OI, Ph-*M*FD, Ph-*SD*rs, and DF-*M*/HDF were the best four features for AF versus AT and AFL classification, in decreasing order, providing an accuracy of 94.74% in the HR layout. Nevertheless, by verifying all combinations among these features, an accuracy of 100% was obtained using only DF-*M*OI and Ph-*FD* for the HR layout, dropping to 94.74% for the LR layout, as shown in Table 1. Also in MC, for AT vs AFL, Ph-*M*SPA, Ph-*M*rs, Ph-*SD*SPA and Ph-Fl*R*, in this order, achieved the highest combined scores, which provided a classification accuracy of 87.50%. By verifying all combinations, it was found that this value can be maintained using only Ph-*M*SPA and Ph-*SD*SPA. For ML, the best feature was DF-pSP and Ph-*SD*rs, with which an accuracy of 78.95% was obtained, and also maintaining its value in the LR layout, although decreasing to 73.68% in two other layouts.

Table 1. Accuracy obtained for each layout.

Leads	AF vs AT/AFL	AT vs AFL	LA vs RA
567 (HR)	100.00%	87.50%	78.95%
252	94.74%	75.00%	73.68%
131	100.00%	75.00%	78.95%
67	94.74%	75.00%	73.68%
64 (LR)	94.74%	87.50%	78.95%

4. Conclusions

This study shows that the three supraventricular cardiac arrhythmias could be distinguished through a reduced number of mechanism related biomarkers, in an in-silico scenario, with high precision, even in layouts with reduced number of leads. Furthermore, this work highlights that metrics which describe "disorganization", such OI and FD, tend to be among the best biomarkers. The noninvasive mechanism location showed reasonable accuracy, due to its complexity. In future analyses, these biomarkers should be tested on data from more complex models and data acquired from patients.

Acknowledgments

VGM is funded by the European Union's Horizon 2020 research and innovation programme under the Marie Skłodowska-Curie grant agreement No. 860974. IS, JAS and JS are supported by grant #2018/25606-2, São Paulo Research Foundation (FAPESP).

References

[1] Page R, et al. 2015 ACC/AHA/HRS guideline for the management of adult patients with supraventricular tachycardia: a report of the American College of Cardiology/American Heart Association Task Force on clinical practice guidelines and the Heart Rhythm Society. Journal of the American College of Cardiology 2016;67(13):e27–e115.

[2] Marques VG, et al. Characterization of atrial arrhythmias in body surface potential mapping: A computational study. Comput Biol Med 2020;127(103904).

[3] Hindricks G, et al. 2020 ESC guidelines for the diagnosis and management of atrial fibrillation developed in collab-

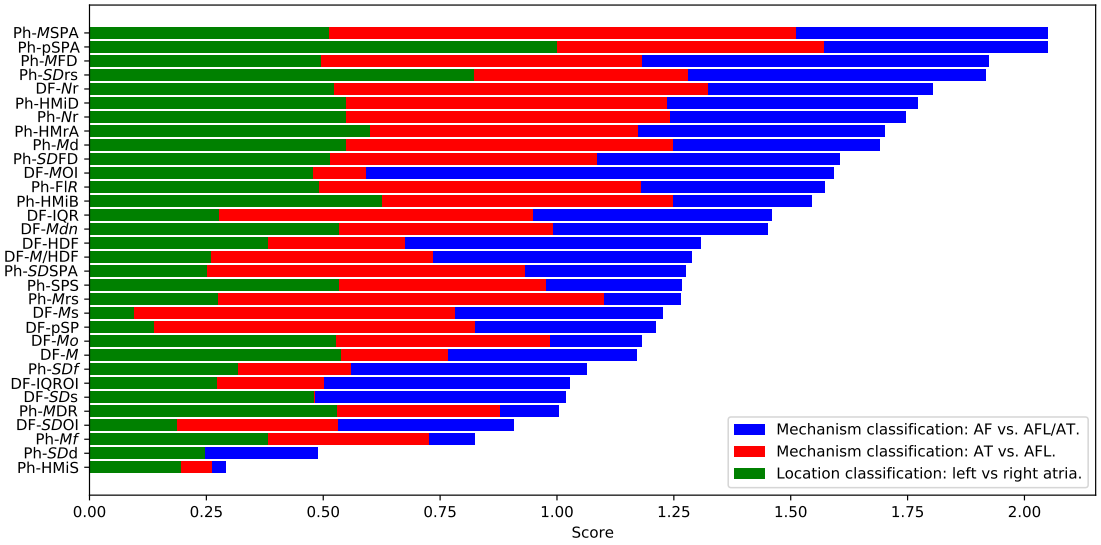

Figure 1. Combined score for each classification task. See sections 2.2 and 2.4 for description of individual features

oration with the european association for Cardio-Thoracic Surgery (EACTS). Eur Heart J 2021;42.

[4] Naser N, et al. The cumulative incidence of stroke, myocardial infarction, heart failure and sudden cardiac death in patients with atrial fibrillation. Med Arch 2017;71.

[5] Salinet J, et al. Electrocardiographic imaging for atrial fibrillation: A perspective from computer models and animal experiments to clinical value. Front Physio 2021;12:488.

[6] Narayan S, et al. Treatment of atrial fibrillation by the ablation of localized sources CONFIRM (conventional ablation for atrial fibrillation with or without focal impulse and rotor modulation) trial. Journal of the American College of Cardiology 2012;60:628–36.

[7] Issa Z, et al. Clinical Arrhythmology and Electrophysiology: A Companion to Braunwald's Heart Disease. Elsevier Health Sciences, 2018.

[8] Rodrigo M, et al. Technical considerations on phase mapping for identification of atrial reentrant activity in direct- and inverse-computed electrograms. Circulation Arrhythmia and Electrophysiology 2017a;10(9).

[9] Dössel AO, et al. Computational modeling of the human atrial anatomy and electrophysiology. Medical Biological Engineering Computing 2012;50(8):773–799.

[10] Liberos A, et al. Phase singularity point tracking for the identification of typical and atypical flutter patients: A clinical-computational study. Computers in Biology and Medicine 2019;104:319–328.

[11] Marques VG, et al. Characterization of atrial arrythmias in body surface potential mapping: A computational study. Computers in Biology and Medicine 2020;127.

[12] Salinet J, et al. Propagation of meandering rotors surrounded by high dominant frequency areas in persistent atrial fibrillation. Heart Rhythm 04 2017;14:–268.

[13] Kuklik P, et al. Reconstruction of instantaneous phase of unipolar atrial contact electrogram using a concept of sinusoidal recomposition and Hilbert transform. IEEE transactions on bio medical engineering 08 2014;62.

[14] Vijayakumar R, et al. Methodology considerations in phase mapping of human cardiac arrhythmias. Circulation Arrhythmia and Electrophysiology 2016;9:e004409.

[15] Canny J. A computational approach to edge detection. Pattern Analysis and Machine Intelligence IEEE Transactions on 1986;PAMI-8:679 – 698.

[16] Kendall M. A new measure of rank correlation. Biometrika 01 1938;30.

[17] Tibshirani R. Regression shrinkage and selection via the Lasso. Journal of the Royal Statistical Society Series B Methodological 01 1996;58:267–288.

Address for correspondence:

Italo Sandoval Ramos de Oliveira
Biomedical Engineering, Universidade Federal do ABC (UFABC)
Alameda da Universidade s/n, Bairro Anchieta,
São Bernardo do Campo, SP, CEP 09606-045, Brazil
italosandova@gmail.com